

Observation of tunable parametric x-ray radiation emitted by laser-plasma electron beams interacting with crystalline structures

A. Curcio¹, M. Ehret¹, J. A. Perez-Hernandez¹, and G. Gatti¹

*Centro de Laseres Pulsados (CLPU), Edificio M5. Parque Científico. C/ Adaja,
8. 37185 Villamayor, Salamanca, Spain*

(Received 14 March 2022; revised 10 June 2022; accepted 21 June 2022; published 28 June 2022)

Parametric x-ray radiation (PXR) is the quantum process analog to Laue diffraction where a pseudophoton is scattered out of a crystalline structure as a radiation photon. In this work, PXR emitted by electron beams generated in a compact laser-plasma accelerator and interacting afterward with a Si 220 crystal is observed in single-shot operations. The combination of laser wakefield acceleration and PXR is an efficient and table-top way to obtain monochromatic, pulsed, ultrashort, and stable emission of high-energy photons: to our knowledge such a complete set of performance parameters is new. Unlike other relevant radiation mechanisms, such as betatron radiation or incoherent bremsstrahlung, PXR is insensitive to the beam energy spread. With a long crystal, we demonstrate the stability of the PXR bandwidth toward shot-to-shot variations of the beam energy and divergence.

DOI: 10.1103/PhysRevAccelBeams.25.063403

The pseudophoton method was introduced by Fermi [1] to study collisions between atoms and charged particles and therefore also to calculate the stopping power of charged particles in dense matter [2]. More specifically, it was developed by Williams [3] to establish the correspondence between collision problems and radiation theory. As is known, the same method was adopted as an approximation by Weizsaker [4] to elegantly approach the quantum electrodynamics (QED) calculations of the bremsstrahlung cross section; finally, it has deserved ample space in the famous books by Jackson [5] and Ter-Mikaelian [6]. In the pseudophoton picture, the particle field is replaced by the photon field. Parametric x-ray radiation (PXR) [7–11] is the process during which pseudophotons carried by the electromagnetic field surrounding a point charge are resonantly scattered out of a crystalline structure as real photons in the direction corresponding to twice the Bragg angle. Indeed, PXR is analog to Laue diffraction, with the difference that the incoming beam is made up of charged particles rather than x rays. However, the interaction of a relativistic charged particle closely resembles the interaction of a plane wave of light, e.g., a photon, for the electromagnetic field around the charge is squeezed in a quasitransverse polarization and propagates almost at the speed of light in vacuum c . Figure 1 shows the diagram corresponding to PXR diffracted by an ultrarelativistic

electron interacting with crystallographic planes. The large momentum transfer during the production of photons with the wave vector $\vec{k} = \omega\vec{v}/v^2 + \vec{g}$ occurs with a recoil \vec{g} received by the crystal. Despite belonging to the group of QED processes in periodic media [12], PXR can also be framed within a classical picture, using the analogy with Laue diffraction. The Hamiltonian density for electromagnetic interactions in the Coulomb gauge is $H = -\vec{j} \cdot \vec{A}$ [13], where the electromagnetic current density is \vec{j} and the radiation potential is $\vec{A} \propto e^{-i\vec{k}\cdot\vec{r}}$, with $\vec{r} = x\hat{x} + y\hat{y} + z\hat{z}$. The current density induced by an electron traveling in a medium can be expressed in terms of the pseudophoton field \vec{E} surrounding the charge, i.e., $\vec{j} = \sigma\vec{E} \propto \chi e^{i\frac{\omega}{v}\vec{v}\cdot\vec{r}}$ [12]. Indeed, the electric conductivity σ is proportional to the electric susceptibility χ [5]. In vacuum $\chi = 0$, thus no radiation is emitted. In a periodic medium (as a single crystal) $\chi \propto e^{i\vec{g}\cdot\vec{r}}$, where \vec{g} is the reciprocal lattice vector which corresponds to a particular set of crystallographic planes. From the microscopic point of view, a wave of electric susceptibility corresponds to a fluid oscillation of the density of carriers in the medium, which can be resonantly driven at specific frequencies and along specific directions fixed by \vec{g} . The interaction rate is calculated through a volume integral of H , yielding a number of scattered photons proportional to $\delta(\vec{k} - \vec{g} - \omega\vec{v}/v^2)$. Such a momentum conservation rule is realized at the vertex in Fig. 1, corresponding to the Laue condition. It's worth noting that in amorphous media, on average $\vec{g} = 0$, then the Laue equation reduces to the Cherenkov condition. In this paper, we report the first observation and characterization of PXR from laser-produced electron beams. Due to its

Published by the American Physical Society under the terms of the [Creative Commons Attribution 4.0 International license](https://creativecommons.org/licenses/by/4.0/). Further distribution of this work must maintain attribution to the author(s) and the published article's title, journal citation, and DOI.

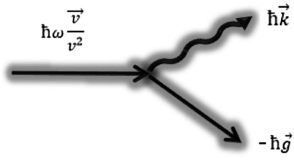


FIG. 1. PXR represented as pseudophoton decay with momentum $\hbar\omega/v$ in a photon and a susceptibility wave.

insensitivity to the beam energy spread, PXR is a suitable candidate for electron-photon conversion in compact laser-plasma accelerators, which notoriously suffer from relatively high beam energy spreads compared to radio-frequency accelerators, especially in the self-injection regime of laser wakefield acceleration [14–23]. Moreover, as demonstrated in this paper, the use of long crystals can aid in the stabilization of the PXR bandwidth, which becomes almost independent of fluctuations of beam energy and divergence. Figure 2 shows the experimental setup and the interaction geometry related to the experimental campaign performed on the VEGA 2 [24] laser system. The electron beam is produced in the self-injection scheme by shooting the 150 TW laser (corresponding to light intensity in the focus of 10^{19} W/cm²) on a supersonic gas-jet composed of pure helium, whose axial profile is characterized via interferometry. The electron plasma density of the laser-produced plasma channel is 3.8×10^{18} cm⁻³. The length of the plasma channel is on average 1.7 mm, characterized by a top image of the formed plasma based on Thomson-scattered light. The transmitted laser energy and the betatron radiation are completely blocked by means of a darkened aluminum foil 200 μ m thick (for the parameters measured in the current

experiment, i.e., electron plasma density, beam energy, and electron divergence, the critical photon energy of the betatron radiation spectrum is expected to be $\lesssim 1$ keV [25]). At the exit of the plasma accelerator, the electron beams pass through a fixed diagnostic station, consisting of an electron spectrometer (to measure the beam energy and energy spread) and a LANEX scintillator (to measure the electron beam divergence and transverse profile). After a complete characterization, the beams are sent into a Si 220 crystal, 30 cm downstream of the plasma, which diffracts the pseudophotons at 90° with respect to the impinging electrons. PXR is detected with a CCD x-ray camera (SOPHIA Ultra-Low-Noise CCD Camera, from Teledyne Princeton Instruments) operated in single-photon counting mode, at 3.75 m from the crystal. A 50 μ m blacked aluminum foil is placed in front of the CCD sensor, for shielding low-energy photons. Due to the self-absorption in the crystal and the background noise in the soft x-ray region affecting the experimental environment, the detection of the first order of diffraction is suppressed. The formation of the second-order diffraction peak is prohibited due to the internal symmetry of the chosen crystal. Therefore, the PXR detection of the third-order diffraction mode is performed, which is centered on the photon energy 13.7 keV. The correct crystal orientation is verified prior to the experiment by means of an x-ray source working in a continuous wave. With the same source, exciting known fluorescence lines (Cu K $_{\alpha}$ and K $_{\beta}$), the CCD camera is calibrated for single-photon counting operations. A spectral resolution of 30 eV is obtained based on the difference (in counts) between the peaks of the fluorescence lines divided by the number of histogram elements (no binning) in that interval. Finally, at the end of the diagnostic chain, a bunch

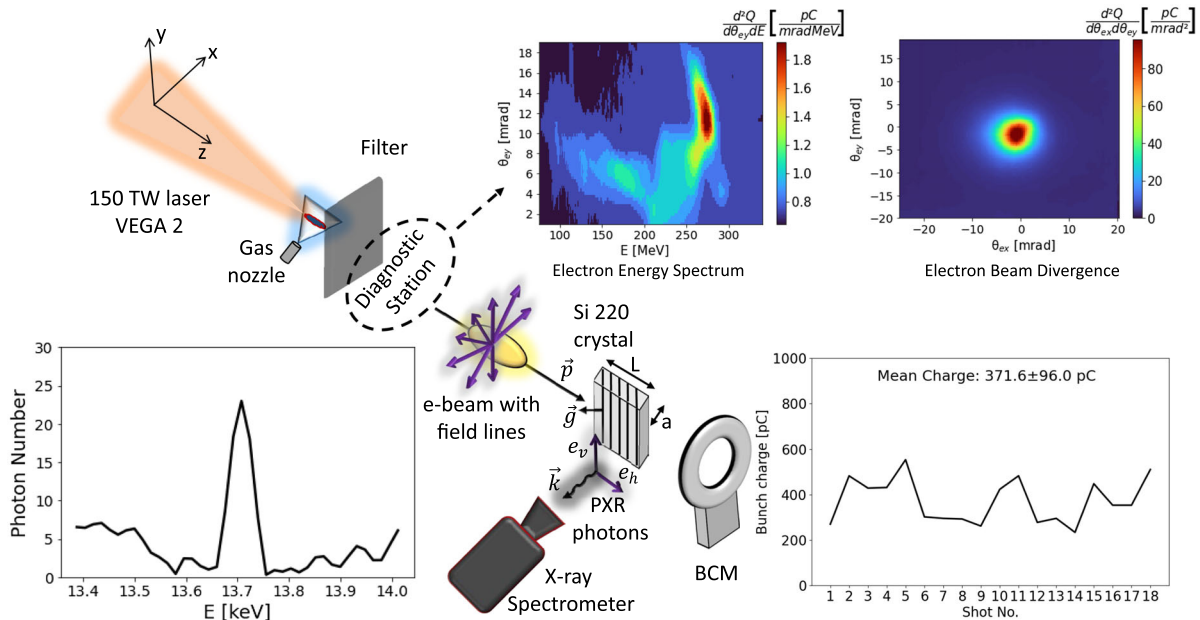


FIG. 2. Experimental setup and geometry for PXR emission by laser-produced electron beams at VEGA 2.

charge monitor (BCM) is placed which measures the charge of the electron beams, in such a way as to determine the PXR quantum efficiency. The effective bunch charge responsible for PXR emission is extrapolated as

$$Q = Q_{\text{BCM}} \int_0^a n(x)T(x)dx, \quad (1)$$

where Q_{BCM} is the bunch charge measured with the BCM and $a = 2$ mm is the length of the side of the crystal. $n(x)$ is the normalized horizontal beam profile obtained at the plane of the crystal (0.9 mm rms). The latter is obtained by averaging the Gaussian fits of the measured beam angular distributions, evaluating the final result at the crystal plane. Finally, $T(x)$ is the Si transmission of x-ray radiation at 13.7 keV for different thicknesses. In fact, the portion of the electron beam closest to the surface facing the detector emits more efficiently than the part of the beam that crosses the crystal along the opposite side, where the PXR photons must pass through a layer of thicker material, undergoing then internal absorption. The beam is aligned with micrometer precision to strike the crystal symmetrically at its center. The factor between Q and Q_{BCM} is found $(9.7 \pm 3.4)\%$, where uncertainty is determined by the shot-to-shot pointing instability. The electron beam passing through the crystal of length $L = 5$ mm is affected by incoherent scattering, increasing its divergence from $\Delta\theta_{e0}$ (shot-to-shot average value 3.1 mrad) to $\Delta\theta_e(z) = \sqrt{\Delta\theta_{e0}^2 + \Delta\theta_{ez}^2}$, in both the x and y directions. The increase in divergence is given by the multiple scattering angle $\Delta\theta_{ez} = (13.6 \text{ MeV}/\gamma[\text{MeV}]) \times \sqrt{z/L_{\text{rad}}[1 + 0.038 \log(z/L_{\text{rad}})]}$ [26], where for silicon $L_{\text{rad}} = 9.37$ cm. In the experimental configuration of this paper, $\Delta\theta_{eL} \simeq 10$ mrad, while the aperture of the detection line is $\Delta\theta_A = 8$ mrad in both planes. The increase in beam size along the crystal is negligible. The choice of

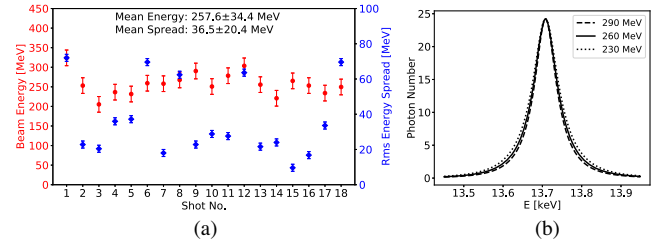


FIG. 3. (a) Shot-to-shot variations of beam energy and energy spread. (b) Simulated PXR line for different beam energies of interest (bunch charge 40 pC).

using a long crystal has been mainly dictated by the need to increase the number of photons on the detector: by doing so, the best value of signal-to-noise ratio approximately equal to 3 has been reached. Nevertheless, the effect of incoherent scattering together with the fixed aperture of the detection line is such to saturate the bandwidth of PXR within the observation angle. In fact, the PXR bandwidth after the propagation of the beam along the crystal is expected to be [12] $\Delta\omega/\omega_B = \min\{\sqrt{1/\gamma_0^2 + \Delta\theta_e^2(L)}, \Delta\theta_A\} \simeq \min\{\Delta\theta_e(L), \Delta\theta_A\} = \Delta\theta_A$, where the average Lorentz factor of the electron beam is γ_0 . This stabilizes the emission with respect to shot-to-shot energy and divergence fluctuations of the electron beam. In practice, the PXR bandwidth stops being sensitive to energy and divergence fluctuations of the electron beam in case that $\Delta\theta_e(L) \gg 1/\gamma_0, \Delta\theta_{e0}$. The stabilization of the bandwidth versus the beam energy fluctuations is described in Fig. 3. The beam energy and energy spread variations in the experiment are reported together with the related shot-to-shot mean value and standard deviation in Fig. 3(a). Simulations of PXR lines for different beam energies in the measured range are shown in Fig. 3(b).

$$\frac{d^3N}{d\theta_h d\theta_v d\omega} = \frac{Qq\omega|\chi|^2}{2\pi\epsilon_0\hbar v c^3} \sum_{s=h,v} \int_0^L dz \int \int d\theta_{ex}\theta_{ey} \Theta(\theta_{ex}, \theta_{ey}; z) \int d\gamma \Gamma(\gamma) \delta(\omega - \omega_B(\gamma)) \left| \frac{\vec{v} \cdot (\vec{\theta} \times \vec{\theta} \times \hat{e}_s)}{\theta_x^2 + \theta_y^2 + \frac{1}{\gamma^2}} \right|^2. \quad (2)$$

The PXR bandwidth stabilization toward divergence fluctuations is also demonstrated by the plots in Fig. 4, where the beam divergence shot-to-shot variations are reported [Fig. 4(a)] alongside simulations of PXR line emission for different initial beam divergence at the entrance of the crystal [Fig. 4(b)]. The simulations of PXR spectra have been performed using Eq. (2), which describes the spectral-angular distribution of PXR at the observation plane [12]. The number of emitted photons is N , q is the electron charge, ϵ_0 is the vacuum dielectric constant, and $\chi = 5.2 \times 10^{-6}$ is the electric susceptibility of the Si crystal at 13.7 keV. The Planck constant is \hbar , v is the electron speed along z , and the unit vectors for the

horizontal and vertical polarizations of PXR are \hat{e}_h and \hat{e}_v , respectively (see Fig. 2). The electron angular and energy distributions are Θ and Γ , respectively. For the calculations of PXR spectra, the angular integration is limited by the aperture of the detection line. The beam angular distribution has been approximated as a bi-Gaussian function with rms size equal to $\Delta\theta_e(z)$ in both angular directions θ_{ex} and θ_{ey} . Therefore, Θ also depends upon z in the sense that it widens due to incoherent scattering: the PXR emitted within the solid angle of observation along the beam path in the crystal is calculated in a self-consistent way. This is confirmed by the fact that both Figs. 3(b) and 4(b) show almost perfect independence

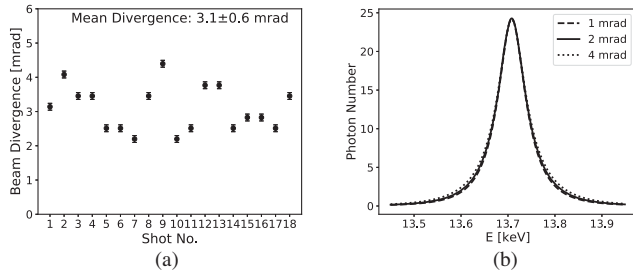


FIG. 4. (a) Shot-to-shot variations of beam divergence. (b) Simulated PXR line for different beam divergences of interest (bunch charge 40 pC).

of the PXR line from the electron beam parameters. The definition $\vec{\theta} = (\theta_h + \cos \theta_B \theta_{ex})\hat{x} + (\theta_v + \cos \theta_B \theta_{ey})\hat{y} + \hat{z}$ has also been used [12], where the Bragg angle in this experiment is $\theta_B = 45^\circ$. The Bragg frequency dependence upon the electron energy is $\omega_B(\gamma) = \omega_{B0}(1 + \Delta\gamma/\gamma_0^3)$ [12], where $\hbar\omega_{B0} = 13.7$ keV, and $\Delta\gamma = \gamma - \gamma_0$ is the Lorentz factor deviation for a particle with Lorentz factor γ . For the present experiment $\Delta\gamma/\gamma_0^3 \simeq 10^{-7}$, hence the repeatability of PXR emission despite large and fluctuating energy spreads. For the sake of completeness, we mention that Γ is obtained from an average of measured electron spectra but does not affect the PXR emission. However, the latter is influenced by charge fluctuations as reported in Fig. 5. Finally, we report observations of PXR fine-tuning (± 0.07 keV) of the central frequency ω_{B0} , limited only by the detector aperture. The tuning has been realized by rotating the crystal around the vertical (y) axis. By definition [12]:

$$\omega_{B0} = \frac{m\pi c}{d \sin \theta_B}, \quad (3)$$

where the lattice constant of Si 220 is $d = 1.92$ Å and here $m = 3$. A tiny rotation of the crystal $d\theta$ shifts the central Bragg frequency as $\omega_{B0} \rightarrow \omega_{B0}(1 - d\theta/\tan \theta_B)$. For $d\theta = \pm 0.3^\circ$, as in this experiment, the photon energy

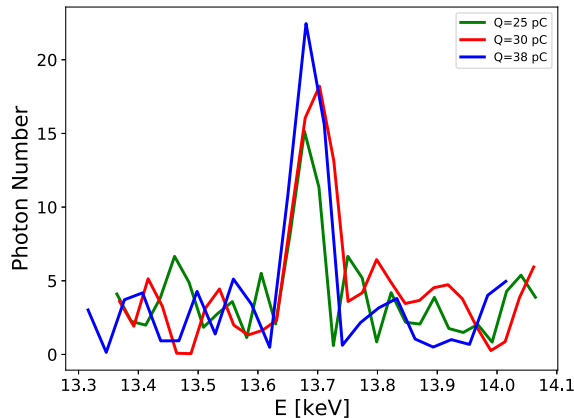


FIG. 5. Shot-to-shot variations of PXR.

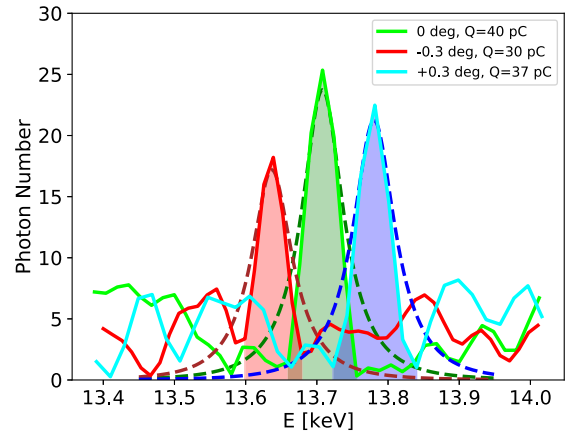


FIG. 6. Fine-tuning of PXR.

13.7 keV is shifted by $\mp 0.5\%$, which is in perfect agreement with the measurements shown in Fig. 6. In conclusion, the first observation of PXR in a compact plasma accelerator is reported. The mean electron-to-photon conversion efficiency has been measured as 3.3×10^{-7} , consistent with previous observations in radio-frequency (rf) accelerators [27]. At this point, we remind the reader that the PXR peak brightness is comparable to the average brightness of a synchrotron light source with an operating energy of 2.5 GeV [12,28]. Due to the extreme shortness of the laser-produced electron bunches [25], monochromatic PXR from such beams is in turn expected to be pulsed and ultrashort. However, the performance of the compact PXR source could be improved by using a different crystal shape and/or refocusing the electron beam in the crystal, and/or simply having the ability to bring the crystal closer to the electron source, or even optimizing the charge per bunch injected in the plasma accelerator. For the experimental configuration of our paper, the use of a wedge-shaped crystal, as the one in Fig. 7, would have improved the x-ray transmission toward the detector by a factor of 7, while using 2 times longer crystal would have doubled the output flux, for overall optimization of the total photon number larger than 1 order of magnitude. Moreover, PXR is a QED mechanism: the authors believe it is important to show that laser-plasma accelerators can be exploited to explore fundamental physics already at the available light intensities [29]. PXR is only one of the beam-crystal interactions implementable with a table-top plasma accelerator: along

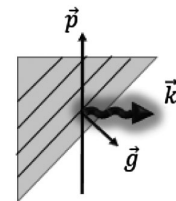


FIG. 7. Optimized crystal shape for a PXR source.

the same new avenue of research in the near future, coherent bremsstrahlung gamma emission and coherent pair production might be demonstrated [6]. In recent times, a PXR source has been realized with materials manipulated at an atomic level, pumped by weakly relativistic electron beams [30]. Our demonstration creates an unprecedented paradigm toward novel photon sources based on compact accelerators. Compared to other mechanisms, PXR is certainly insensitive to large energy spreads of the electron beams and thus also to their fluctuations. Furthermore, the use of long crystals increases the photon number while also stabilizing the radiation bandwidth toward shot-to-shot variations of energy and divergence.

ACKNOWLEDGMENTS

The research leading to these results has received funding from LASERLAB-EUROPE V (Grant Agreement No. 871124, European Union Horizon 2020 research and innovation program).

-
- [1] E. Fermi, Über die theorie des stoßes zwischen atomen und elektrisch geladenen teilchen, *Z. Phys.* **29**, 315 (1924).
- [2] E. Fermi, The ionization loss of energy in gases and in condensed materials, *Phys. Rev.* **57**, 485 (1940).
- [3] E. J. Williams, *Correlation of Certain Collision Problems with Radiation Theory* (Levin & Munksgaard, Denmark, 1935).
- [4] C. Von Weizsacker, Radiation emitted in collisions of very fast electrons, *Z. Phys.* **88**, 95 (1934).
- [5] J. Jackson, *Classical Electrodynamics*, 2nd ed. (John Wiley & Sons, New York, 1975).
- [6] M. L. Ter-Mikaelian, *High-Energy Electromagnetic Processes in Condensed Media* (John Wiley & Sons, New York, 1972), Vol. 29.
- [7] A. Shchagin, V. Pristupa, and N. Khizhnyak, A fine structure of parametric x-ray radiation from relativistic electrons in a crystal, *Phys. Lett. A* **148**, 485 (1990).
- [8] X. Artru and P. Rullhusen, Parametric x-rays and diffracted transition radiation in perfect and mosaic crystals, *Nucl. Instrum. Methods Phys. Res., Sect. B* **145**, 1 (1998).
- [9] H. Nitta, Kinematical theory of parametric x-ray radiation, *Phys. Lett. A* **158**, 270 (1991).
- [10] K.-H. Brenzinger, B. Limburg, H. Backe, S. Dambach, H. Euteneuer, F. Hagenbuck, C. Herberg, K. Kaiser, O. Kettig, G. Kube *et al.*, How Narrow is the Linewidth of Parametric X-Ray Radiation?, *Phys. Rev. Lett.* **79**, 2462 (1997).
- [11] W. Scandale, G. Arduini, R. Assmann, F. Cerutti, S. Gilardoni, J. Christiansen, E. Laface, R. Losito, A. Masi, E. Metral *et al.*, Observation of parametric x-rays produced by 400 GeV/c protons in bent crystals, *Phys. Lett. B* **701**, 180 (2011).
- [12] V. G. Baryshevsky, I. D. Feranchuk, and A. P. Ulyanenko, *Parametric X-ray Radiation in Crystals: Theory, Experiment and Applications* (Springer Science & Business Media, the Netherlands, 2005), Vol. 213.
- [13] E. G. Harris, *A Pedestrian Approach to Quantum Field Theory* (Courier Corporation, USA; Canada, 2014).
- [14] B. Pollock, C. Clayton, J. Ralph, F. Albert, A. Davidson, L. Divol, C. Filip, S. Glenzer, K. Herpoldt, W. Lu *et al.*, Demonstration of a Narrow Energy Spread, 0.5 GeV Electron Beam from a Two-Stage Laser Wakefield Accelerator, *Phys. Rev. Lett.* **107**, 045001 (2011).
- [15] G. Li, Q. Ain, S. Li, M. Saeed, D. Papp, C. Kamperidis, and N. A. Hafz, Control of electron beam energy-spread by beam loading effects in a laser-plasma accelerator, *Plasma Phys. Controlled Fusion* **62**, 055004 (2020).
- [16] I. Kostyukov, E. Nerush, A. Pukhov, and V. Seredov, Electron Self-Injection in Multidimensional Relativistic-Plasma Wake Fields, *Phys. Rev. Lett.* **103**, 175003 (2009).
- [17] R. Hu, H. Lu, Y. Shou, C. Lin, H. Zhuo, C.-e. Chen, and X. Yan, Brilliant GeV electron beam with narrow energy spread generated by a laser plasma accelerator, *Phys. Rev. Accel. Beams* **19**, 091301 (2016).
- [18] J. Faure, C. Rechatin, A. Norlin, A. Lifschitz, Y. Glinec, and V. Malka, Controlled injection and acceleration of electrons in plasma wakefields by colliding laser pulses, *Nature (London)* **444**, 737 (2006).
- [19] C. Thauray, E. Guillaume, A. Lifschitz, K. Ta Phuoc, M. Hansson, G. Grittani, J. Gautier, J.-P. Goddet, A. Tafzi, O. Lundh *et al.*, Shock assisted ionization injection in laser-plasma accelerators, *Sci. Rep.* **5**, 16310 (2015).
- [20] S. Barzegar and A. R. Niknam, Laser pulse-electron beam synergy effect on electron self-injection and higher energy gain in laser wakefield accelerators, *Sci. Rep.* **11**, 37 (2021).
- [21] M. Vargas, W. Schumaker, Z.-H. He, Z. Zhao, K. Behm, V. Chvykov, B. Hou, K. Krushelnick, A. Maksimchuk, V. Yanovsky *et al.*, Improvements to laser wakefield accelerated electron beam stability, divergence, and energy spread using three-dimensional printed two-stage gas cell targets, *Appl. Phys. Lett.* **104**, 174103 (2014).
- [22] S. Y. Kalmykov, A. Beck, S. Yi, V. Khudik, M. C. Downer, E. Lefebvre, B. A. Shadwick, and D. Umstadter, Electron self-injection into an evolving plasma bubble: Quasi-monoenergetic laser-plasma acceleration in the blowout regime, *Phys. Plasmas* **18**, 056704 (2011).
- [23] T. Tajima and J. M. Dawson, Laser Electron Accelerator, *Phys. Rev. Lett.* **43**, 267 (1979).
- [24] L. Volpe, R. Fedosejevs, G. Gatti, J. Pérez-Hernández, C. Méndez, J. Apiñaniz, X. Vaisseau, C. Salgado, M. Huault, S. Malko *et al.*, Generation of high energy laser-driven electron and proton sources with the 200 TW system VEGA 2 at the Centro de Laseres Pulsados, *High Power Laser Sci. Eng.* **7**, e25 (2019).
- [25] A. Curcio and G. Gatti, Time-domain study of the synchrotron radiation emitted from electron beams in plasma focusing channels, *Phys. Rev. E* **105**, 025201 (2022).
- [26] V. L. Highland, Some practical remarks on multiple scattering, *Nucl. Instrum. Methods* **129**, 497 (1975).
- [27] A. Didenko, B. Kalinin, S. Pak, A. Potylitsin, S. Vorobiev, V. Baryshevsky, V. Danilov, and I. Feranchuk, Observation of monochromatic x-ray radiation from 900 MeV electrons

- transmitting through a diamond crystal, *Phys. Lett. A* **110**, 177 (1985).
- [28] A. Thompson, D. Attwood, E. Gullikson, M. Howells, K.-J. Kim, J. Kirz, J. Kortright, I. Lindau, P. Pianetta, A. Robinson *et al.*, *X-ray Data Booklet* (Lawrence Berkeley National Laboratory, University of California, Berkeley, CA, 2001).
- [29] T. Tajima and G. Mourou, Zettawatt-exawatt lasers and their applications in ultrastrong-field physics, *Phys. Rev. ST Accel. Beams* **5**, 031301 (2002).
- [30] M. Shencis, A. K. Budniak, X. Shi, R. Dahan, Y. Kurman, M. Kalina, H. Herzig Sheinflux, M. Blei, M. K. Svendsen, Y. Amouyal *et al.*, Tunable free-electron x-ray radiation from van der Waals materials, *Nat. Photonics* **14**, 686 (2020).